Journal of Ceramic Processing Research. Vol. 24, No. 6, pp. 977~982 (2023)
(Received 3 September 2023, Received in revised form 9 October 2023, Accepted 28 October 2023)
https://doi.org/10.36410/jcpr.2023.24.6.977

J O U R N A L O F
Ceramic Processing Research

Microwave dielectric properties of $Li_3Mg_2SbO_5F_2$ oxyfluorides ceramics produced by reaction-sintering method

Pengshen Wu[a], Cuijin Pei[a], Miao Chen[a], Xu Gao[a], Weihong Liu[b], Guoguang Yao[a,*] and Jin Liu[c]
[a]*School of Science, Xi'an University of Posts and Telecommunications, Xi'an 710121, China*
[b]*School of Electronic Energineering, Xi'an University of Posts and Telecommunications, Xi'an 710121, China*
[c]*School of Fine Arts, Shaanxi Normal University, Xi'an, 710062, China*

By a reaction-sintering approach $Li_3Mg_2SbO_5F_2$ oxyfluorides ceramics were prepared. The sinterability, microstructure, phase transition along with microwave dielectric performances of present ceramics were researched. A gradual phase transition from cubic to orthorhombic in $Li_3Mg_2SbO_5F_2$ ceramics sintered above 825 °C was identified by XRD refinement analysis. The microwave dielectric performances of present ceramics were closely correlated with its phase transition process and microstructure. Typically, optimal microwave dielectric performances (ε_r ~ 8.1, τ_f ~ –54.0 ppm/°C, $Q \times f$ ~ 68,500 GHz (under 9.2 GHz)) were achieved for 825 °C-sintered $Li_3Mg_2SbO_5F_2$ ceramics. Moreover, a cylindrical dielectric resonator antenna fabricated from $Li_3Mg_2SbO_5F_2$ ceramics exhibited a maximum return loss (S_{11}) of –30.3 dB, a maximum gain of 5.3 dB and VSWR of 1.1 at the center frequency of 11.6 GHz, and impedance bandwidth of 300 MHz (at –10 dB), respectively.

Keywords: Ceramics, $Li_3Mg_2SbO_5F_2$ oxyfluorides, microwave dielectric properties, antenna

Introduction

The urge of 5G/6G technology is proliferation for its low latency. To accomplish the low latency, dielectric ceramics with a low dielectric constant ($\varepsilon_r \leq 10$) is internal demand to reduce latency of the components [1]. Simultaneously, a high quality factor (Q×f), an approximating zero resonant frequency temperature coefficient (τ_f), and an inherent low sintering temperature (below 950 °C) are also the essential requires for microwave dielectric ceramics, which is beneficial for lower signal attenuation, better environment stability and further cost reduction [2-4]. Thus, immense attentions have been pay to develop new dielectric ceramics with above performances concurrently.

Recently, researchers started to enlarge new microwave dielectric ceramics from oxides to oxyfluorides-containing LiF. It was reported that the partial chemical fluorination (O^{2-} is replaced with F^-) not only decrease the sintering temperature, but also reduce the ε_r of oxides ceramics [5]. For instance, a series of oxyfluorides ceramics such as $Li_{2+x}Mg_{1-x}Ti_3O_{8-x}F_x$ (τ_f = -6.0 ppm/°C, Qf = 55,000 GHz, ε_r=24.8, fired at 1100 °C), Li_3TiO_3F (Qf = 96, 200 GHz, ε_r=17.3, τ_f = -32.7 ppm/°C, fired at 900 °C), Li_4NbO_4F (Qf = 61,100 GHz, ε_r=15.2, τ_f = -51.0 ppm/°C, fired at 825 °C), Li_4MgNbO_5F (Q×f = 93,000 GHz, ε_r=15.5, and τ_f = -40.0 ppm/◦C, fired at 900 °C), $Li_8Mg_xTi_3O_{9+x}F_2$ (Q×f = 119,700 GHz, ε_r=16.8, τ_f = -41.6 ppm/°C, fired at 875 °C) were reported, which exhibited promising microwave dielectric properties and inherit low sintering temperature [6-8]. The chemical fluorination turns out to be an effective approach for remarkable lowering the sintering temperature of oxides ceramics [9, 10]. In these oxyfluorides ceramics-containing LiF, two distinct low temperature sintering mechanisms have been invoked: one is connected with liquid phase sintering caused by the low melting point of LiF (845 °C), the other is due to the reduced chemical potential caused by F^- substitution for O^{2-} ions; or both [11-13]. However, consensus about the sintering mechanism of oxyfluorides ceramics using LiF as fluorine source. To explore the exact sintering mechanism of the oxyfluorides ceramics, a new oxyfluoride ceramics, namely $Li_3Mg_2SbO_5F_2$, was designed using high melting point MgF_2 (1250 °C) instead of LiF as reactive source of fluorine [14]. In present paper, we demonstrate the possibility to fabricate $Li_3Mg_2SbO_5F_2$ by reaction sintering route. The effects of using MgF_2 as fluorine source on the sinterability, phase constitutions, microstructure and dielectric properties in microwave frequency for $Li_3Mg_2SbO_5F_2$ ceramics were systematically investigated. Besides, a cylindrical dielectric resonator antenna (CDRA) was manufactured and measured from $Li_3Mg_2SbO_5F_2$ for X-band applications.

*Corresponding author:
Tel : +86 29 88166089
Fax: +86 29 88166333
E-mail: yaoguoguang@xupt.edu.cn

Experimental

The raw materials are high-purity powders: Sb_2O_3 (99.0%, Guo Yao Co., Ltd.), MgF_2 (99.99%, Aladdin), Li_2CO_3 (98.0%, Guo Yao Co., Ltd.), and MgO (99.9%, Guo Yao Co., Ltd.). According to stoichiometric $Li_3Mg_2SbO_5F_2$, the starting materials were weighed followed by milling for 8 h in ethanol. The milling powders were stoved, then granulated and molded, finally sintered for 5 h (800 °C-875 °C). The specific reaction sintering process has been described in our former work [15].

By Archimedes' drainage method, the apparent densities in $Li_3Mg_2SbO_5F_2$ sintered bodies were evaluated. The crystal structure as well as phase transition were measured using powder X-ray diffraction (PXRD, PANalytical) at ambient temperature. PXRD data were collected in a 2θ region of 5-100° with a step size of 0.015°. The microstructural morphology for fired ceramics was examined via a scanning electron microscope. The antenna performances along with microwave dielectric performances of present samples were estimated via a Rohde & schwarz network analysis (ZVB20, Germany). In the temperature region of 25-85 °C, the τ_f had been determined via the following formula:

$$\tau_f = \frac{f_{85} - f_{25}}{f_{25} \times (85 - 25)} \quad (1)$$

The cylindrical dielectric resonator antenna (CDRA) was designed using the High-Frequency Structure Simulator software.

Results and Discussion

The dense degree of $Li_3Mg_2SbO_5F_2$ ceramics were evaluated via radial shrinkage and apparent density (ρ_{ap}). Fig. 1 illustrates the ρ_{ap} and radial shrinkage of $Li_3Mg_2SbO_5F_2$ ceramics sintered at 800-875 °C. As seen in Fig. 1, both the ρ_{ap} and radial shrinkage exhibited the similar variational tendency with the increase of firing

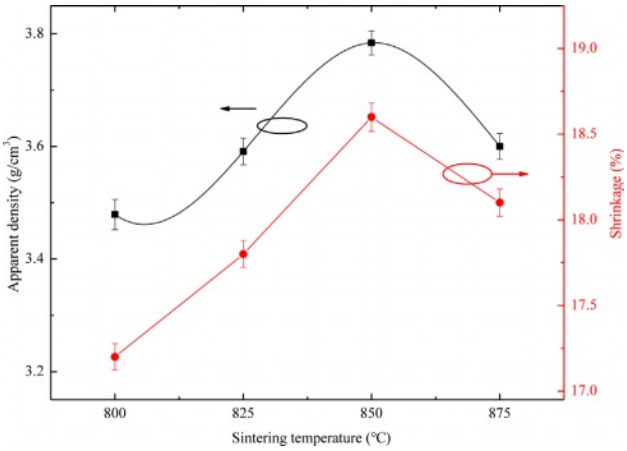

Fig. 1. Apparent density and radial shrinkage of $Li_3Mg_2SbO_5F_2$ ceramics sintered at 800-875 °C.

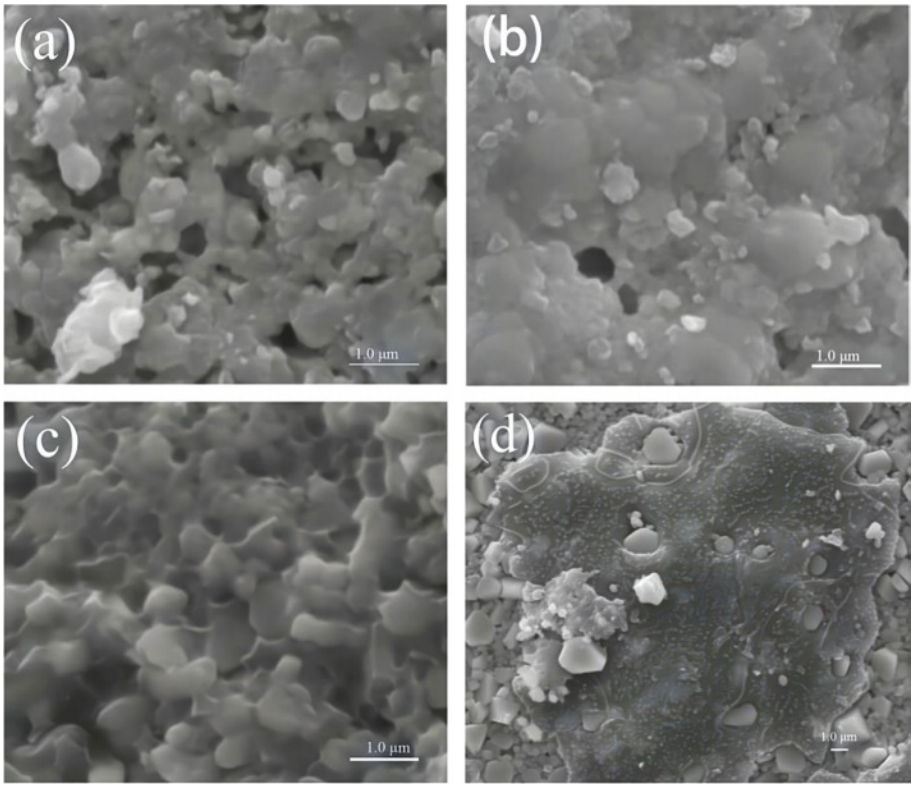

Fig. 2. SEM photographs at different sintering temperature of $Li_3Mg_2SbO_5F_2$ ceramics: (a) 800 °C, (b) 825 °C, (c) 850 °C, (d) 875 °C.

temperature. As the firing temperature increased, both the ρ_{ap} and radial shrinkage initially increased, reached their respective maximum values at 850 °C, and then declined. As the heating temperature increase, the enhancement of ρ_{ap} for $Li_3Mg_2SbO_5F_2$ ceramics was due to the reduction of internal pores, while its abatement was due to over-sintering, which was consistent with the microstructure observation intuitively as discussed below.

The typical SEM photographs at different sintering temperature of $Li_3Mg_2SbO_5F_2$ ceramics are exhibited in Fig. 2. Some intergranular pores were observed for 775 °C-sintered sample, corresponding to its relatively lower ρ_{ap}, as seen in Fig. 2(a) and Fig. 1. The number of intergranular pores vanished gradually in line with enhancement of firing temperature, and a relative uniformly dense microstructure were achieved for 850 °C-sintered sample. When the firing temperature reached 875 °C, a residual liquid phase wrapped grains was appeared due to over-sintered, which would result in an adverse effect on present ceramics' density and dielectric performances [16].

Fig. 3 gives the XRD profiles of $Li_3Mg_2SbO_5F_2$ ceramics sintered under 800-875 °C. The main diffraction peaks of 775 °C and 800 °C-sintered samples individually matched well with the standard PDF cards of Mg_2PtO_4 (#77-0017) with a cubic rock salt structure and $Li_3Mg_2SbO_6$ (#87-0652) with an orthorhombic rock salt structure, and some tiny peaks matched well with the standard PDF card of MgO (#78-0430). When the sintering temperature exceeded 825 °C, the trace phase of MgO vanished, and the content of $Li_3Mg_2SbO_6$ phase increased with augment of sintering temperature, indicating that partial cubic phase transformed to an orthorhombic phase. This structural transformation was also found in previous studies [8], which may influence present ceramics' dielectric properties [17, 18].

To further identify the detailed structure information along with quantity of each phase, the Rietveld refinements of XRD data of $Li_3Mg_2SbO_6F_2$ samples were conducted. Fig. 4 illustrates the fitted and measured XRD profiles using cubic Mg_2PtO_4 and orthorhombic

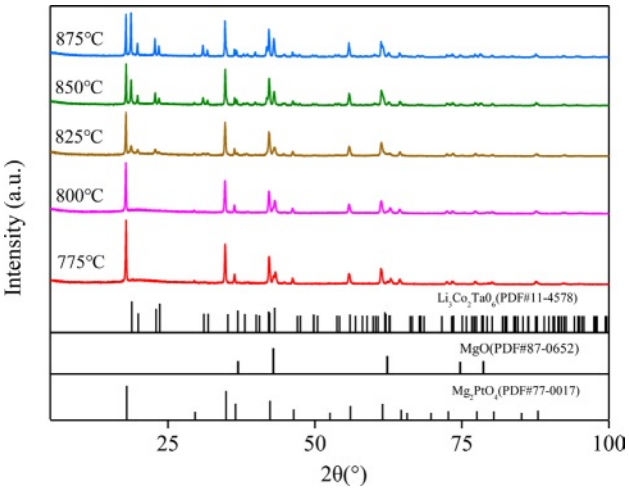

Fig. 3. XRD patterns of $Li_3Mg_2SbO_5F_2$ ceramics sintered at 800-875 °C.

$Li_3Mg_2SbO_6$ as initial models, the detailed refinement results are summarized in Table 1. A good match between the fitted and measured diffraction patterns along with low reliability factors suggested the structure model and refined results were creditable. From Table 1, the quantity of orthorhombic structural phase increased from 40.1 to 61.8%, with an enhancement of sintering temperature from 825 to 875 °C.

The plots of ε_r and τ_f of $Li_3Mg_2SbO_5F_2$ ceramics with various heating condition are exhibited in Fig. 5. With augment of heating temperature, the ε_r rose first and achieved a saturation value around 8.6 at 850 °C and subsequently declined. Evidently, the ε_r and ρ_{ap} exhibited a similar variational tendency with the sintering temperature, which suggested the ε_r is deeply linked with the ρ_{ap}. Moreover, in the temperature range of 800-875 °C, the τ_f retained steady at -53 ppm/°C regardless of the sintering temperature, although the phases transferred from cubic to orthorhombic.

Fig. 6 shows the dependence of the Q×f in $Li_3Mg_2SbO_5F_2$ ceramics on sintering temperature. The tendency variation of Q×f was initially rose from the

Table 1. Refinement results of $Li_3Mg_2SbO_5F_2$ ceramics sintered at 800-875 °C.

S.T.	Phase structure	a (Å)	b (Å)	c (Å)	Phase content (wt.%)	R_p(%)	R_{wp}(%)
800	Cubic	8.5378(7)	8.5378(7)	8.5378(7)	99.0	8.69	12.15
	Cubic	4.1772(6)	4.1772(6)	4.1772(6)	1.0		
825	Orthorhombic	5.8853(4)	8.6939(7)	17.7300(6)	40.1	9.72	12.85
	Cubic	8.5364(5)	8.5364(5)	8.5364(5)	59.9		
850	Orthorhombic	5.9333(5)	8.6406(4)	17.8389(4)	43.9	10.58	14.56
	Cubic	8.5385(8)	8.5385(8)	8.5385(8)	56.1		
875	Orthorhombic	5.9355(8)	8.6333(6)	17.8310(4)	61.8	10.65	14.83
	Cubic	8.5405(3)	8.5405(3)	8.5405(3)	38.2		

S.T.: sintering temperature

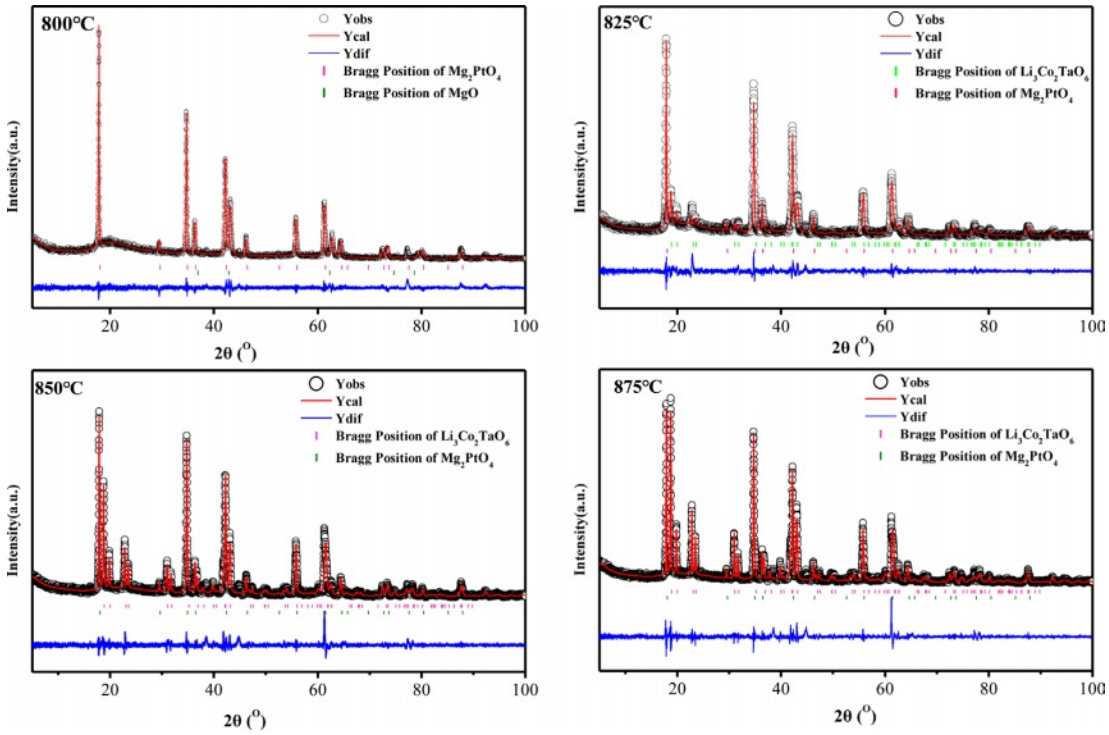

Fig. 4. Rietveld refinement profiles of $Li_3Mg_2SbO_5F_2$ sintered at 800-875 °C.

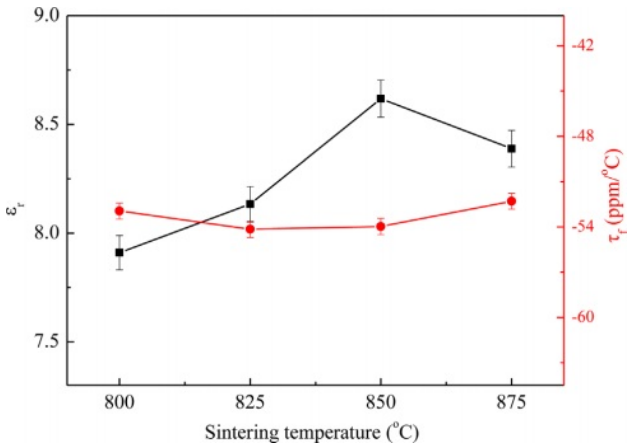

Fig. 5. The plots of ε_r and τ_f in $Li_3Mg_2SbO_5F_2$ ceramics with sintering temperature.

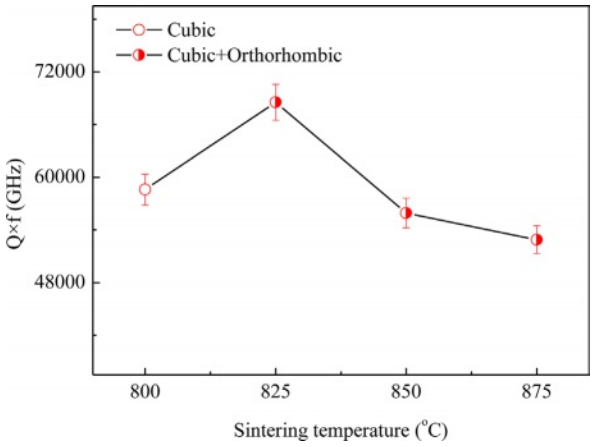

Fig. 6. Q×f curve of $Li_3Mg_2SbO_5F_2$ ceramics with sintering temperature.

onset of 58,600 GHz at 800 °C to a maximum value of 68500 GHz at 825 °C, and then decreased gradually to 52800 GHz at 875 °C. The tendency of variation of Q×f was somewhat different from ρ_{ap} versus sintering temperature, indicating others factor except ρ_{ap} that could affect the $Li_3Mg_2SbO_5F_2$ ceramics' Q×f. Overall, the Q×f is determined by inherent factors (like ordering, symmetry, and phonon vibration) and extrinsic factors (like pores, inclusions and distortion) [19-21]. For given ceramics with high symmetry showed a high *Qxf* due to its high structural stability [22]. In our cases, the initial improvement of Q×f was due to the reduce of pores (seen Fig. 2). Subsequently, the degradation of Q×f was attributed to the increased content of orthorhombic phase with low symmetry (seen Table 1) , and the reduce of ρ_{ap} (seen Fig. 1) owing over-sintering. The similar effect of phase transition on Q×f was also reported by Ohsato et al. [23].

Feasibility evaluation of $Li_3Mg_2SbO_5F_2$ ceramics serving as CDRAs in X-band range is demonstrated. The sketch, prototype and final optimized parameters of $Li_3Mg_2SbO_5F_2$-based CDRA are displayed in Fig. 6(a)-(c). Fig. 6(d) displays the numerical and measured reflection characteristics (S_{11}) curves of the $Li_3Mg_2SbO_5F_2$ CDRA. The numerical S_{11} of -32.7 dB at central frequency of 11.4 GHz has an impedance bandwidth of 1.3 GHz (10.8-12.1 GHz) compared to the measured S_{11} of -38.5 dB at 11.6 GHz with an

Table 2. CDRA performances comparison of different dielectric ceramics for X-band applications

Composition	f (GHz)	Bandwidth (MHz)	S_{11} (dB)	Gain (dB)	VSWR	Reference
Al_2O_3	8.6	390	-20.3	3.9	1.2	25
$BaTiO_3/V_2O_5$	9.5	226	-20.0	8.2	-	26
95MCT	9.58	560	-15.4	-	-	27
LTMN0.25	10.02	175	-36.0	5.4	-	28
$Li_3Mg_2SbO_5F_2$	11.6	300	-30.3	5.3	1.1	this work

*-: not mentioned

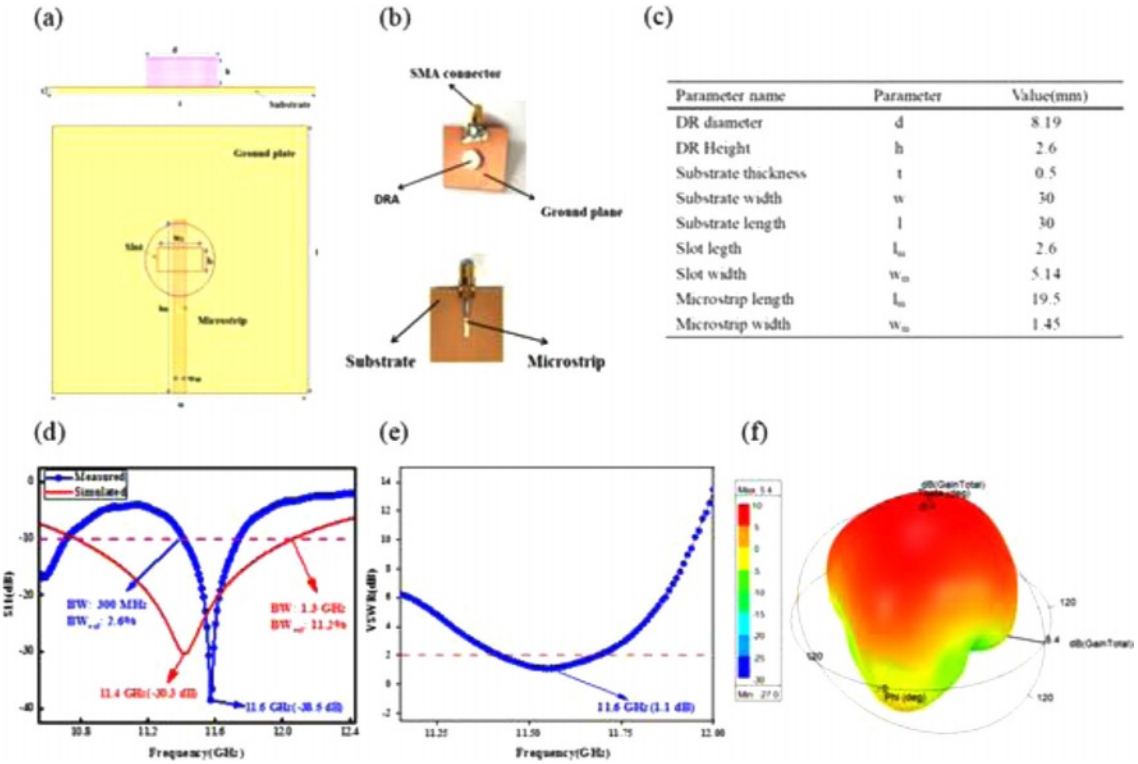

Fig. 7. The schematic (a) and prototype (b) of simulated and fabricated CDRA, (c) optimized parameter values, (d) simulated and tested return loss (S_{11}), (e) tested voltage standing wave ratio (VSWR), and (f) simulated 3D radiation pattern at 11.6 GHz.

impedance bandwidth of 300 MHz (11.4-11.7 GHz). The above mismatch in central frequency, S_{11} along with antenna bandwidth of the simulated and fabricated antenna are due to the fabrication process's preciseness, tiny position alteration of DR, and SMA connector's welding, etc [24]. As presented in Fig. 6(e), the measured VSWR of CDRA was 1.1 at 11.6 GHz and below 2 within the bandwidth of 300 MHz (11.4-11.7 GHz). Fig. 6(f) presents the numerical three-dimensional gain plot of the simulated antenna, which showed a maximum gain of 5.4 dB along Z direction. Table 2 gives CDRA performances made of different dielectric ceramics for X-band applications. From Table 2, our $Li_3Mg_2SbO_5F_2$ CDRA displays comparable antenna performances with that of other CDRAs. Moreover, it points out that our CDRA displays a very good trade-off between gain, bandwidth and return loss (S_{11}).

Conclusions

Microwave dielectric performances and evolution of phase structure of $Li_3Mg_2SbO_5F_2$ ceramics prepared by reactive sintering method have been reported. A phase transition from cubic to orthorhombic occurred at above 825 °C as identified by XRD refinement analysis. The phase transition process and microstructure take a vital effect on the microwave dielectric performances of present ceramics. Typically, 825 °C-sintered $Li_3Mg_2SbO_5F_2$ specimens exhibited microwave dielectric performances ($\varepsilon_r \sim 8.1$, $\tau_f \sim -54.0$ ppm/°C, $Q \times f \sim 68{,}500$ GHz (under 9.2 GHz)). Moreover, a cylindrical dielectric resonator antenna made from $Li_3Mg_2SbO_5F_2$ ceramics

was designed for X-band applications, which exhibited return loss (S_{11}) of -38.5 dB, gain of 5.4 dB, VSWR of 1.1, and -10 dB bandwidth of 300 MHz at the center frequency of 11.6 GHz, respectively.

Acknowledgements

The authors acknowledge supports from National Natural Science Foundation of China (Grant Nos. 52002317, 52272122), Xi'an Sciences Plan Project (No. 2021XJZZ0075), and Undergraduate Innovation and Entrepreneurship Training Program in China (No. 202211664020).

References

1. T.H. Hsu, C.L. Huang, Mat. Sci. Semicon. Proc. 158 (2023) 107355.
2. J. Liu, B. Liu, C.C. Hu, Q.W. Zhou, K.X. Song, J. Eur. Ceram. Soc. 43[14] (2023) 6130-6136.
3. Y.S. Park, E.S. Kim, J. Ceram. Process. Res. 23[6] (2022) 920-926.
4. S. Kim, C.B. Hong, S.H. Kwon, S.O. Yoon, J. Ceram. Process. Res. 18[6] (2017) 421-424.
5. S.H. Han, Y.N. Li, F.Y. Hao, H. Zhou, S.L. Qi, G.F. Tian, D.Z. Wu, Eur. Polym. J. 143 (2021) 110206.
6. X. Chu, J. Jiang, J.Z. Wang, Y.C. Wu, L. Gan, T.J. Zhang, Ceram. Int. 47[3] (2021) 4344-4451.
7. P. Zhang, M.M. Yang, M. Xiao, Z.T. Zheng, Mater. Chem. Phys. 236 (2019) 121805.
8. Z.X. Wang, Y.F. Guo, J.M. Li, C.H. Li, Ceram. Int. 49 (2023) 33425-33431.
9. K. Xiao, C.C. Li, Y. Tang, Y.F. Tian, C.Z. Yin, J.Q. Chen, J. Li, L. Duan, H.C. Xiang, L. Fang, J. Alloys. Compd. 835 (2020) 155320.
10. L.M. Huang, J.J. Bian, J. Eur. Ceram. Soc. 43[15] (2023) 6893-6899.
11. X.H. Zhang, Y.M. Ding, J.J. Bian, J. Mater. Sci-Mater. El. 28 (2017) 12755-12760.
12. A. Kan, R. Hirabayashi, S. Takahashi, H. Ogawa, Ceram. Int. 49[6] (2023) 9883-9892.
13. W. Jin, J.J.Tan, J.X. Yan, Y. Tao, N.N. Yao, X.M. Ruan, Pei, C.J. J. Ceram. Process. Res. 22[6] (2021) 675-678.
14. X.L. Fan, J.T. Fan, K.C. Qian, Z.Y. Shen, L.L. Zhang, B.X. Jiang, T. Feng, L. Zhang, J. Eur. Ceram. Soc. 15 (2022) 7203-7208.
15. G.G. Yao, J. Ceram. Process. Res. 16[1] (2015) 41-44.
16. S.O. Yoon, S. Kim, Y.H. Kim, S.J. Kim, S.M. Jeong, J. Ceram. Process. Res. 17[10] (2016) 1024-1027.
17. X. Zhang, Z.X. Fang, H.Y. Yang, P. Zhao, X. Zhang, Y.P. Li, Z. Xiong, H.C. Yang, S.R. Zhang, B. Tang, Acta. Mater. 206 (2021) 116636.
18. X. Zhang, Z.X. Fang, Z. Xiong, H.Y. Yang, S.R. Zhang, B. Tang, J. Phys. Chem. C. 124 (2020) 22069-22081.
19. H. Ohsato, J. Varghese, H.L. Jantunen, Electromagnetic Materials and Devices, 2020: 1-26.
20. E. Schlömann, Phys. Rev. 135 (1964) 412-418.
21. Y.M. Ding, J.J. Bian, Mater. Res. Bull. 48 (2013) 2776-2781.
22. H. Ohsato, J. Varghese, H. Jantunen, Electromagnetic Materials and Devices, 3 (2020).
23. H. Ohsato, J. Varghese, A. Kan, J.S. Kim, I. Kagomiy, H. Ogawa, M.T. Sebastian, H. Jantunen, Ceram. Int. 47[2] (2021) 2735-2742.
24. R. Madhuri, A. Rajan, S. Ganesanpotti, Mater. Res. Bull. 158 (2023) 112069.
25. A. Sharma, K. Khare, S.C. Shrivastava, Electronics and Instrumentation Engineering 2 (2013) 2247-2252.
26. R. Chandran, C.O. Sreekala, S.K. Menon, Materials Today: Proceedings 33 (2020) 1367-1370.
27. Y.C. Chen, S.M. Tsao, C.S. Lin, S.C. Wang, Y.H. Chien, J. Alloy. Compd. 471 (2009) 347-351.
28. H.H. Guo, D. Zhou, C. Du, J. Mater. Chem. C 8 (2020) 4690-4700.